PERGAMON

International Journal of Multiphase Flow 26 (2000) 1305–1324

International Journal of Multiphase Flow

www.elsevier.com/locate/ijmulflow

Particle drift in the field of internal gravity wave ☆

S.A. Grinshpun [a,*], Yu.N. Redcoborody [b], S.G. Kravchuk [b], V.I. Zadorozhnii [b], V.I. Zhdanov [b]

[a] *Aerosol Research and Exposure Assessment Laboratory, Department of Environmental Health, University of Cincinnati, P.O. Box 670056, Cincinnati, OH 45267-0056, USA*

[b] *Astronomical Observatory, Kyiv Shevchenko University, Observatorna St., 3, Kyiv-53, 254053, Ukraine*

Received 23 April 1998; received in revised form 27 July 1999

Abstract

Similarly to an acoustic wave, an internal gravity wave (IGW) can cause the drift of a dispersed component in a two-component system, e.g. in a hydrosol or an aerosol. The IGW-caused particle drift may play a significance role in many natural processes occurring in very large water reservoirs or air volumes and thus is of interest for atmospheric and oceanic research. The analytical and numerical calculations of the IGW-caused particle drift motion were performed in this study for the following two sets of conditions: (i) propagating IGW in a horizontal infinite waveguide and (ii) standing IGW in a rectangular resonator. It was shown that particles concentrate in certain areas of an IGW field as a result of their migration. When IGW is propagating in an infinite waveguide, the particle drift causes the vertical stratification and horizontal unidirectional motion. The particle size affects the shape of the particle trajectories and the vertical component of the drift velocity in an infinite waveguide. In contrast, the shape of trajectories in the IGW rectangular resonator is not affected by the particle size and IGW intensity. The IGW-caused particle drift was shown to result in purification of a two-component system or in its "structurization" (the formation of purified areas of the fluid alternating with the areas loaded with particles). These effects were found to be low energy consuming: $\sim$10 J/m^3 of liquid. However, the particle migration in the infinite waveguide and rectangular resonator is a very slow process, and the time needed for an efficient purification of a fluid increases quickly with the decrease of particle size. The particle coagulation is expected to significantly accelerate the fluid purification. Another way to reduce this characteristic time is proposed through utilizing the horizontal component of the particle drift in the semi-infinite IGW waveguide. © 2000 Elsevier Science Ltd. All rights reserved.

Keywords: Internal gravity wave; Suspension; Particle drift; Structurization; Waveguide

☆ One of the authors, Dr. Yurij Redcoborody, who initiated the study died in Kyiv, Ukraine, when the paper preparation was at its final stage. It was due to his effort that this research became possible.

* Corresponding author.

0301-9322/00/$ - see front matter © 2000 Elsevier Science Ltd. All rights reserved.
PII: S0301-9322(99)00091-9

1. Introduction

The particle motion in a fluid caused by an acoustic field includes a wave-generated oscillation and a slow drift of the particles. Depending on the type of the acoustic wave, particles are concentrated in certain regions of the acoustic field or/and exhibit unidirectional motion (Bergman, 1957; Mednikov, 1963). For example, in the case of a one-dimensional standing acoustic wave, the drift favors the stratification of multiphase media so that the particles move to the planes where oscillation amplitude reaches its maximum or minimum value (King, 1934). Standing acoustic waves have been extensively used for precipitation of particles from highly-concentrated aerosol systems because they promote intensive particle coagulation. In the case of a propagating (traveling) acoustic wave, the unidirectional particle drift emerges along with the transversal drift stratification. This allows the particle extraction from liquids and gases regardless of their coagulation rate and thus makes the extraction efficiency essentially independent on the particle concentration in the fluid. The acoustic drift has been studied by King (1934) for the standing and propagating waves. The King's theory can be applied to sufficiently large particles (the particle Reynolds number $Re_p \gg 1$), when the so-called radiation pressure force F is determined primarily by inertial properties of the fluid. In this case, F is proportional to dV_{rel}/dt, where V_{rel} is the particle velocity with respect to the fluid. The acoustic drift of relatively small particles ($Re_p \ll 1$), for which the fluid viscosity effect is essential and F is proportional to V_{rel}, has been studied by Westervelt (1950), Duhin (1960), Vainstein et al. (1992) and Redcoborody (1995). It has been shown that the particles migrate to the nodes of the one-dimensional standing acoustic wave (Duhin, 1960; Vainstein et al., 1992), while the propagating wave causes homogeneous particle migration in the wake of the wave (Westervelt, 1950; Redcoborody, 1995).

The internal gravity wave (IGW) that has been observed in the earth and solar atmospheres (Gossard and Hooke, 1975; Priest, 1984) and in the ocean (Lighthill, 1978) is characterized by much lower frequency (e.g., about 10^{-2} Hz, Lighthill, 1978). While the restoring force for an acoustic wave is caused by the pressure gradient, the IGW is associated with the buoyancy force (i.e., the difference between the Arhimedus and the gravity forces). The word "internal" is used to differentiate the IGW from a surface gravity wave (SGW) which propagates along the interface surface between two fluids (Landau and Lifshitz, 1986). The IGW may affect a two-component system by causing the particle drift motion, similarly to the acoustic wave. As IGW has significantly greater wavelength and much smaller group velocity compared with the acoustic wave, the particle extraction from liquids and gases due to the gravity wave drift is expected to be efficient and low energy consuming. The extremely low frequency of IGW makes the limitation of $Re_p \ll 1$ justified for various applications of the particle drift effect in suspensions and aerosols. In this situation the fluid viscosity effect is predominant while the particle inertia effect is negligibly small. Although IGW is generally associated with very large fluid volumes (in the order of 100 m or km), it may be excited in a waveguide or a resonator in a characteristic dimensions as low as several meters (Stevenson, 1973).

In this study, we investigated the drift of spherical particles in a liquid caused by the two-dimensional IGW. The drift characteristics were determined analytically and numerically for the two-dimensional horizontal infinite waveguide (propagating wave) and the rectangular

resonator (standing wave). It was shown that the particles migrate and concentrate in certain areas of the IGW field which may lead to the purification of suspensions due to structurization of these two-component systems. This effect appeared to be low energy consuming, but the migration velocity in the resonator and its vertical component in the infinite waveguide were found to be very low. Thus, the fluid purification process (associated with its structurization) is very slow, especially for relatively small particles because the time needed for an efficient purification increases quickly with the decrease of particle size. When propagating in the infinite waveguide, IGW causes vertical stratification which is accompanied by the horizontal unidirectional motion of particles with considerable rate. This rate was shown not to be affected by the particle size. The method of accelerating the IGW-caused structurization is introduced and evaluated in this study through utilizing the horizontal component of the particle drift in the semi-infinite waveguide.

2. Basic equations

2.1. Spherical particle under viscous force

The motion of an essentially inertialess particle ($Re_p \ll 1$) in a continuous medium is governed by the Stokes law (Batchelor, 1967)

$$F = 6\pi\nu\rho R_p V_{rel}. \tag{1}$$

where ν and ρ are the fluid kinematic viscosity and density, respectively, and R_p is the particle radius. Since it is assumed that the particle density ρ_p is approximately equal to the density ρ of the liquid, the buoyancy force (which is proportional to R_p^3) becomes negligibly small. If the size of a spherical particle is significantly smaller than the characteristic space scale, the particle motion equation is

$$m_p\ddot{\boldsymbol{r}} = K_p\big[\boldsymbol{V}(\boldsymbol{r}, t) - \dot{\boldsymbol{r}}\big], \tag{2}$$

where $K_p = 6\pi\nu\rho R_p$; $\boldsymbol{V}(\boldsymbol{r}, t)$ is the liquid velocity at point $\boldsymbol{r}$, where the particle is located, and m_p is the particle mass. This model is applicable when the particles suspended into a liquid have approximately the same density as this liquid, i.e. the buoyancy force is neglected. In two-dimensional case the components of Eq. (2) are

$$\tau_p\ddot{x} + \dot{x} = V_x(x, z, t); \tag{3}$$

$$\tau_p\ddot{z} + \dot{z} = V_z(x, z, t), \tag{4}$$

where

$$\tau_p = \frac{2}{9}\frac{\rho_p R_p^2}{\nu\rho}. \tag{5}$$

2.2. Internal gravity wave

To describe the wave-like two-dimensional motion in the ideal fluid exposed to the uniform gravity field, the standard hydrodynamic equations (Lighthill, 1978) are utilized as follows:

$$\rho_0 \frac{\partial u}{\partial t} = -\frac{\partial p'}{\partial x}; \tag{6}$$

$$\rho_0 \frac{\partial w}{\partial t} = -\frac{\partial p'}{\partial z} - g\rho'; \tag{7}$$

$$\frac{\partial \rho'}{\partial t} + \rho_0 \left(\frac{\partial u}{\partial x} + \frac{\partial w}{\partial z} \right) + w \frac{\mathrm{d}\rho_0}{\mathrm{d}z} = 0; \tag{8}$$

$$\frac{\partial p'}{\partial t} + w \frac{\mathrm{d}p_0}{\mathrm{d}z} = c_0^2 \left(\frac{\partial \rho'}{\partial t} + w \frac{\mathrm{d}\rho_0}{\mathrm{d}z} \right) \tag{9}$$

These equations are linearized with respect to initial state which is described as

$$\boldsymbol{V}_0 \equiv 0;\ p_0 = p_0(z);\ \rho_0 = \rho_0(z);\ \nabla p_0 = \rho_0 \boldsymbol{g};\ T_0 = \text{const};\ p' \equiv p - p_0;\ \rho' \equiv \rho - \rho_0. \tag{10}$$

Here the subscript 0 represents the liquid undisturbed by the wave; u and w are horizontal and vertical components of the velocity $\boldsymbol{V}$, respectively; x and z are the axes directed horizontally and vertically (upward), respectively; c_0 is the sound speed.

As the parameters of Eqs. (6)–(9) are not dependent on the time t and on the x-coordinate, these differential equations can be simplified to a system of algebraic equations. After solving this system with respect to w, the inverse Fourie transformation leads to the following single equation:

$$\frac{\partial^2}{\partial t^2} \left[\Delta w - \frac{1}{H_0} \frac{\partial w}{\partial z} \right] + N^2 \frac{\partial^2}{\partial x^2} w - \frac{1}{c_0^2} \frac{\partial^4 w}{\partial x^4} = 0 \tag{11}$$

Here

$$H_0 \equiv -\left(\frac{1}{\rho_0} \frac{\mathrm{d}\rho_0}{\mathrm{d}z} \right)^{-1}; \tag{12}$$

N is the so-called Brunt-Väisälä frequency (Lighthill, 1978):

$$N \equiv \left[-\frac{g}{\rho_0} \frac{\mathrm{d}\rho_0}{\mathrm{d}z} - \frac{g^2}{c_0^2} \right]^{1/2}. \tag{13}$$

Similarly,

$$\frac{\partial^2 u}{\partial x^2} - \frac{1}{gH_0}\frac{\partial^2 u}{\partial t^2} - \frac{1}{g}\frac{\partial^3 w}{\partial x \partial t^2} - \frac{1}{H_0}\frac{\partial w}{\partial x} + \frac{1}{g}\frac{\partial^3 u}{\partial z \partial t^2} + \frac{\partial^2 w}{\partial x \partial z} = 0. \tag{14}$$

The solution of Eqs. (11) and (14) for the low-frequency small scale IGW can be expressed in the following form

$$w(x, z, t) = \hat{w}(x, z)\mathrm{e}^{-i\omega t} \tag{15}$$

where

$$\omega \leq N, \tag{16}$$

$$\lambda_x, \lambda_z \ll H_0, \tag{17}$$

λ_x and λ_z are the horizontal and vertical wavelengths, respectively. Due to the conditions expressed in Eqs. (16) and (17), the second and the third terms of Eq. (11) are negligibly small. Thus, in the case of a low-frequency small-scale IGW, Eq. (11) is simplified as

$$\frac{\partial^2}{\partial t^2}\Delta w + N^2\frac{\partial^2}{\partial x^2}w = 0. \tag{18}$$

Similarly,

$$\frac{\partial u}{\partial x} = -\frac{\partial w}{\partial z}. \tag{19}$$

3. IGW-caused particle drift in horizontal infinite waveguide

3.1. Analytical model

The two-dimensional IGW is considered in a horizontal waveguide of the infinite length and limited height. Assuming that the liquid fills a waveguide with horizontal rigid boundaries, the boundary conditions for $w(x, z, t)$ are

$$w|_{z=0} = w|_{z=h} = 0, \tag{20}$$

where h is the waveguide height. After substituting Eq. (15) into Eq. (18), we have

$$\hat{w}_{zz} + \left(1 - \frac{N^2}{\omega^2}\right)\hat{w}_{xx} = 0. \tag{21}$$

From Eqs. (20), (21) and (15), (19), respectively, the vertical w_n and horizontal u_n components of the liquid velocity in the n-th mode can be obtained as

$$w_n(x, z, t) = -Ck\sin\left(\frac{\pi n}{h}z\right)\sin(kx - \omega_n t) \tag{22}$$

and

$$u_n(x, z, t) = -C\frac{\pi n}{h}\cos\left(\frac{\pi n}{h}z\right)\cos(kx - \omega_n t) \tag{23}$$

Here k is a horizontal wavenumber and frequency ω_n is determined by

$$\omega_n^2 = N^2\frac{k^2}{k^2 + \pi^2 n^2/h^2}; \tag{24}$$

$n = 1, 2, 3, \ldots$; value C is an arbitrary constant. Eqs. (22) and (23) show that the IGW in a horizontal waveguide of the infinite length and limited height represents the composition of the transversal standing wave and longitudinal propagating wave.

Substituting (22) and (23) in (4) and (3), respectively, the nonlinear equations of the particle motion in the IGW field are obtained in a non-dimensional form as

$$\alpha\eta'' + \eta' = -\beta \sin\eta \sin(\xi - \theta) \tag{25}$$

and

$$\alpha\xi'' + \xi' = -\beta \cos\eta \cos(\xi - \theta). \tag{26}$$

Here

$$\xi \equiv kx,\ \eta \equiv \frac{\pi n}{h}z,\ \theta \equiv \omega_n t \tag{27}$$

and

$$\alpha \equiv \omega_n \tau_p, \quad \beta \equiv \frac{Ck\pi n}{h\omega_n} \tag{28}$$

are non-dimensional variables (ξ, η, and θ) and parameters (α and β); τ_p is determined by Eq. (5). In the case of the linear approximation of the IGW, i.e.,$\beta \ll 1$, the solutions of the set of nonlinear non-autonomic Eqs. (25) and (26) can be obtained with the sufficient accuracy in the following form (Kapitza, 1951)

$$\xi(\theta) = \xi_0(\theta) + \xi_1(\theta); \quad \eta(\theta) = \eta_0(\theta) + \eta_1(\theta), \tag{29}$$

where $\xi_1$and η_1 are small perturbations oscillating with the period 2π whereas ξ_0 and η_0 are slow drift components of the particle motion, $|\xi_1(\theta)| \prec\prec |\xi_0(\theta)|$, $|\eta_1(\theta)| \prec\prec |\eta_0(\theta)|$. The functions $\xi_1(\theta)$ and $\eta_1(\theta)$ can be obtained as solutions of Eqs. (26) and (25), respectively. To derive the equations for $\xi_0(\theta)$ and $\eta_0(\theta)$ the right-hand sides of (25) and (26) are expanded in powers of ξ_1 and η_1 taking into account the first order terms only:

$$\alpha\eta_0'' + \eta_0' + \alpha\eta_1'' + \eta_1' = -\beta\big(\sin\eta_0 + \eta_1\cos\eta_0\big)\big[\sin(\xi_0 - \theta) + \xi_1\cos(\xi_0 - \theta)\big] \tag{25a}$$

and

$$\alpha\xi_0'' + \xi_0' + \alpha\xi_1'' + \xi_1' = -\beta\big(\cos\eta_0 - \eta_1\sin\eta_0\big)\big[\cos(\xi_0 - \theta) - \xi_1\sin(\xi_0 - \theta)\big] \tag{26a}$$

The two terms of each equation, representing an oscillation and a smooth variation, respectively, can be mutually cancelled.

Separating the oscillating terms, we obtain that

$$\alpha\eta_1'' + \eta_1' = -\beta \sin\eta_0 \sin(\xi_0 - \theta) \tag{25b}$$

$$\alpha\xi_1'' + \xi_1' = -\beta \cos\eta_0 \cos(\xi_0 - \theta) \tag{26b}$$

When integrating, η_0 are ξ_0 treated as constants. The right-hand sides of Eqs. (25b) and (26b) are modified utilizing the following expressions: $2i\sin(\xi_0 - \theta) = \exp[i(\xi_0 - \theta)] - \exp[-i(\xi_0 - \theta)]$ and $2\cos(\xi_0 - \theta) = \exp[i(\xi_0 - \theta)] + \exp[-i(\xi_0 - \theta)]$, where $i = \sqrt{-1}$. Both equations are further modified using $\exp(\theta/\alpha)$ as a multiplying factor. Thus,

$$\eta_1(\theta) = C_1 + C_2\exp(-\theta/\alpha) - \frac{\left[\beta \sin\eta_0 \cos(\xi_0 - \theta) - \alpha\beta \sin\eta_0 \sin(\xi_0 - \theta)\right]}{(1+\alpha^2)} \tag{25c}$$

and

$$\xi_1(\theta) = C_3 + C_4\exp(-\theta/\alpha) + \frac{\left[\beta \cos\eta_0 \sin(\xi_0 - \theta) + \alpha\beta \cos\eta_0 \cos(\xi_0 - \theta)\right]}{(1+\alpha^2)} \tag{26c}$$

where C_1, C_2, C_3, and C_4 are constant. If $\theta \gg \alpha$, $C_2\exp(-\theta/\alpha)$ and $C_4\exp(-\theta/\alpha)$ are both neglected.

The above expressions of $\eta_1(\theta)$ and $\xi_1(\theta)$ are used in Eqs. (25a) and (26a) to obtain the smooth variation terms. The equations are then averaged over 2π interval of θ ($\eta_0(\theta)$ and $\xi_0(\theta)$ are treated as constants). This leads to the following equations of the particle drift in the field of the IGW:

$$\alpha\eta_0'' + \eta_0' = -\frac{\alpha\beta^2}{2(1+\alpha^2)}\sin(2\eta_0) \tag{30}$$

and

$$\alpha\xi_0'' + \xi_0' = \frac{\beta^2}{2(1+\alpha^2)}\cos(2\eta_0). \tag{31}$$

It is evident that for $\beta \ll 1$ the characteristic time of the particle drift is much greater than the period of oscillations, i.e. the non-dimensional time scale τ_* of the functions $\xi_0(\theta)$ and $\eta_0(\theta)$ is sufficiently large:

$$\tau_* \gg 2\pi. \tag{32}$$

If particles up to 1 mm in size are dispersed in a water suspension ($\tau_p \leq 10^{-1}$ s) and the IGW frequency is $\omega_n \sim N \sim (10^{-3}\text{–}10^{-1})$ s^{-1} (see Lighthill, 1978), then

$$\alpha = \omega_n\tau_p \ll 1. \tag{33}$$

Conditions (32) and (33) allow us to neglect the first terms of the left-hand sides of Eqs. (30)

and (31) and due to this fact the particle drift equations are reduced to

$$\eta_0' = -\frac{\alpha\beta^2}{2(1+\alpha^2)}\sin(2\eta_0) \tag{34}$$

and

$$\xi_0' = \frac{\beta^2}{2(1+\alpha^2)}\cos(2\eta_0). \tag{35}$$

Eq. (34) describes the vertical drift motion, while Eq. (35) describes the combination of the vertical and horizontal ones.

The expression for the vertical drift velocity (Eq. (34)) has the following equilibrium points:

$$\eta_{0m} = \frac{\pi}{2}m, \quad m = 0, 1, \ldots, 2n \tag{36}$$

For the even m-values, Eq. (36) represents attractive planes while for the odd values it represents repelling planes. The general solution of Eq. (34) can be found in the following form:

$$\cos 2\eta_0 = \frac{1 - C_0 \exp(-2A\theta)}{1 + C_0 \exp(-2A\theta)}, \tag{37}$$

where

$$A \equiv \frac{\alpha\beta^2}{1+\alpha^2}; \quad C_0 \equiv \frac{1 - \cos 2\eta_0(0)}{1 + \cos 2\eta_0(0)} \tag{38}$$

In particular, if $0 < \eta_0(0) < \pi/2$, then

$$\eta_0(\theta) = \frac{1}{2}\cos^{-1}\left[\frac{1 - C_0 \exp(-2A\theta)}{1 + C_0 \exp(-2A\theta)}\right] \tag{39}$$

At $\theta \to +\infty$ the particles migrate to the bottom of the waveguide: $\eta_0(\theta) \to 0$.

The vertical particle drift in the horizontal waveguide results in the particle stratification. The characteristic non-dimensional time of the stratification (the time interval needed for the particle to reach the vicinity of the nearest attractive plane), can be estimated using Eq. (38) that at $\alpha \ll 1$ reads as

$$\tau_* \sim \frac{1}{A} \sim \frac{1}{\alpha\beta^2}. \tag{40}$$

Hence, the particles concentrate near the attractive planes $\eta_0 = \pi s$ ($s = 0, 1, \ldots, n$) with the mean velocity that is proportional to the square of the particle size (see Eqs. (5) and (28)) and to the IGW intensity (see Eqs. (22) and (28)).

Eq. (35) for the horizontal drift motion can be integrated if the vertical drift component is known (see Eqs. (37) and (39)). If the particle has reached the attractive plane due to its

vertical drift, then the solution of Eq. (34) reads

$$\eta_0(\theta) \cong \pi s, \quad s = 0, 1, \ldots, n, \tag{41}$$

and the solution of Eq. (35) reads

$$\xi_0(\theta) \cong C_1 + \frac{\beta^2}{2(1+\alpha^2)}\theta, \tag{42}$$

where C_1 is an arbitrary constant. Eq. (42) represents the unidirectional uniform particle drift in the horizontal direction with the following non-dimensional velocity:

$$\Lambda = \frac{\mathrm{d}\xi_0}{\mathrm{d}\theta} = \frac{\beta^2}{2(1+\alpha^2)}. \tag{43}$$

It is concluded that if $\alpha \ll 1$ (which represents a typical situation of the dispersed system exposed to the IGW, see Eq. (33)), the horizontal drift velocity does not essentially depend on the particle size and is determined only by the parameters of the waveguide and the IGW (see Eq. (28)).

The particle drift trajectories $\eta_0(\xi_0)$ can be found when Eq. (34) is divided by Eq. (35) so that $\mathrm{d}\eta_0/\mathrm{d}\xi_0 = -\alpha[\tan(2\eta_0)]$. The general solution of this equation is

$$\sin\left[2\eta_0(\xi_0)\right] = \left[\sin\left(2\eta_0(0)\right)\right]\exp(-2\alpha\xi_0), \tag{44}$$

where $\eta_0(0) = \eta_0|_{\xi_0=0}$. In particular, when $0 < \eta_0(0) < \pi/4$, the particle trajectory is described by the following equation

$$\eta_0(\xi_0) = \frac{1}{2}\sin^{-1}\left[\sin\left(2\eta_0(0)\right)\right]\exp(-2\alpha\xi_0). \tag{45}$$

The trajectories of particles initially located at points (0; $\pi/4$) and (0; $3\pi/4$) in the IGW-mode with $n = 1$ were found from Eq. (44). The calculations were conducted for the two fractions of particles of a unit density dispersed in a water suspension and exposed to the IGW with $\omega = 10^{-1}$ s^{-1} ($N = 10^{-1}$ s^{-1}): $R_p = 100$ μm ($\alpha \sim 10^{-4}$) and 500 μm ($\alpha \sim 10^{-3}$). The results are shown in Fig. 1. It is seen that the shape of the particle trajectory essentially depends on the value of α, i.e., on the particle size, see Eqs. (28) and (5). The figure also shows that the particle migration from the repelling plane to the nearest attractive plane becomes more efficient with the increase in α. This effect is explained by the fact that the vertical drift velocity in the waveguide is proportional to α (see Eq. (34)), whereas the horizontal velocity does not depend on α at $\alpha \ll 1$ (see Eq. (35)).

3.2. Computer simulation

The results presented above were obtained through analytical solution of nonlinear Eqs. (25) and (26); this solution was found as a result of the approximation of the particle motion by Eq. (29) at $\beta \ll 1$. In order to further explore the IGW-caused particle drift motion and

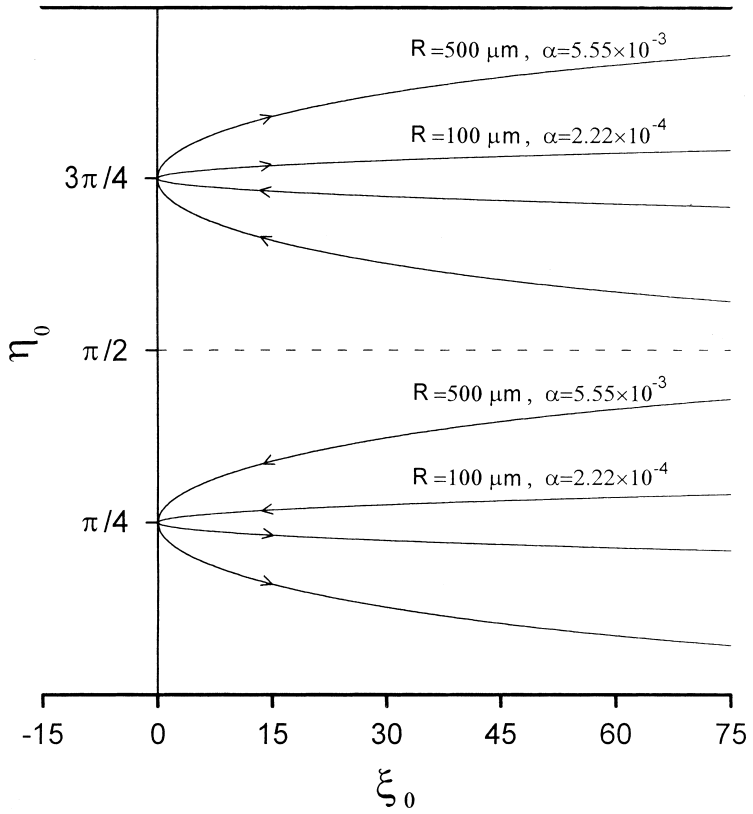

Fig. 1. Particle trajectories in the horizontal infinite IGW waveguide (analytical calculation).

evaluate the above approximations, the computer simulation of the IGW-caused particle motion in the horizontal waveguide was performed.

The Cauchy problem that includes the nonlinear non-autonomic Eqs. (25) and (26) subjected to the initial conditions, described as $\theta = 0$, $\xi(0) = 0$, $\eta(0) = \pi/4$, $\xi'(0) = \eta'(0) = 0$, was numerically solved using the Runge-Kutta algorithm of the 4th order with the fixed stepsize. The following parameters were used: $\beta = 10^{-1}$; $\alpha = 10^{-4}$; 10^{-3}; 10^{-2}; 10^{-1}; 1. The stepsize was chosen through several iterations; the total absolute error was not to exceed 10^{-6}. To control the accuracy of this numerical solution, some additional numerical simulations were performed using the fifth order Runge-Kutta algorithms with the Merson remainder term. The computations started at $\eta = \pi/4$ and were interrupted at $\eta = 10^{-4}$.

The numerical simulation data obtained as the time-dependent functions, $\eta(\theta)$, are shown in Fig. 2. The results represent the superposition of the two components: the oscillation motion and the drift motion of the particles in the field of the IGW (the oscillation pattern is shown on the figure). Fig. 2 demonstrates that the liquid get purified with the time due to the particle migration to the bottom of the waveguide (at $n = 1$). If $n > 1$, the two-component system develops some specific structure as the particles concentrate near the attractive planes. However, the vertical drift appears to be a very slow process, especially for relatively small

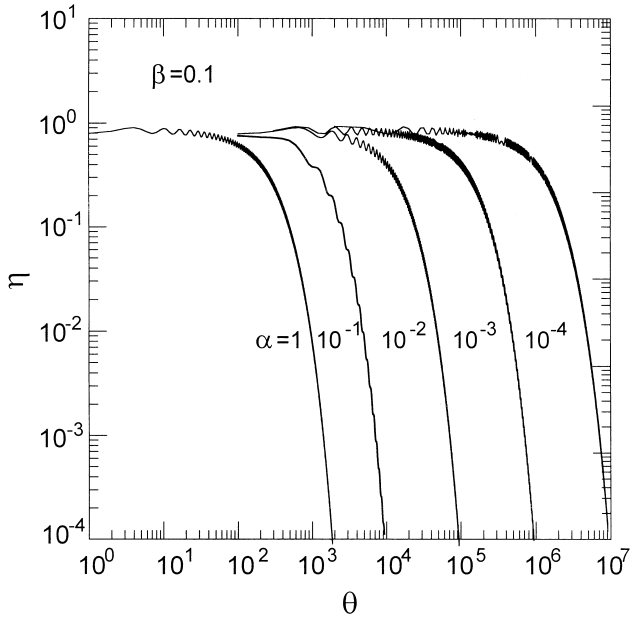

Fig. 2. Particle verticle drift with the time in the horizontal infinite IGW waveguide (numerical calculation).

particles ($\alpha \ll 1$). For instance, the time needed for the entire purification of the water suspension with particles of 100–500 μm due to the IGW-caused vertical drift can be as long as several days.

The data obtained numerically were averaged by eliminating the oscillation component and then compared with the results obtained analytically in Eq. (39). The numerical and analytical values agreed with each other very well: e.g., the difference in η-values did not exceed 1% for $\alpha = 1$, β ranging from 0.01 to 0.1, and $\theta > \tau_*$.

4. IGW-caused particle drift in two-dimensional rectangular resonator

4.1. Analytical model

Assuming that the liquid fills a two-dimensional rectangular resonator ($L \times h$) with rigid boundaries, the boundary conditions are

$$w|_{z=0} = w|_{z=h} = 0; \quad u|_{x=0} = u|_{x=L} = 0. \tag{46}$$

The IGW velocity field in the resonator can be calculated using Eqs. (15)–(19) and (21) as

$$w_{nm}(x, z, t) = C \sin\left(\frac{\pi n}{h} z\right) \cos\left(\frac{\pi m}{L} x\right) \cos(\omega_{nm} t) \tag{47}$$

and

$$u_{nm}(x, z, t) = -C\left(\frac{L}{h}\frac{n}{m}\right)\cos\left(\frac{\pi n}{h}z\right)\sin\left(\frac{\pi m}{L}x\right)\cos(\omega_{nm}t) \tag{48}$$

Here frequency ω_{nm} is determined as

$$\omega_{nm}^2 = N^2\frac{m^2/L^2}{m^2/L^2 + n^2/h^2}; \tag{49}$$

$m, n = 1, 2, 3, \ldots$; C is an arbitrary constant. Eqs. (47) and (48) show that the IGW-mode in the resonator represents the combination of the vertical and horizontal standing waves.

Substituting (47) and (48) in (4) and (3), respectively, and introducing the non-dimensional variables

$$\xi \equiv \frac{\pi m}{L}x; \quad \eta \equiv \frac{\pi n}{h}z; \quad \theta \equiv \omega_{nm}t \tag{50}$$

and parameters

$$\alpha \equiv \omega_{mn}\tau_p; \quad \beta \equiv \frac{C\pi n}{h\omega_{nm}}, \tag{51}$$

the equations of the particle motion in the rectangular IGW resonator are obtained as

$$\alpha\eta'' + \eta' = \beta \sin\eta \cos\xi \cos\theta \tag{52}$$

and

$$\alpha\xi'' + \xi' = -\beta \cos\eta \sin\xi \cos\theta. \tag{53}$$

Similarly to the solution found for the waveguide at $\beta \ll 1$, the equations for the particle drift components in the rectangular resonator are

$$\alpha\eta_0'' + \eta_0' = -\frac{\alpha\beta^2}{2(1+\alpha^2)}\sin\eta_0 \cos\eta_0 \tag{54}$$

and

$$\alpha\xi_0'' + \xi_0' = -\frac{\alpha\beta^2}{2(1+\alpha^2)}\sin\xi_0 \cos\xi_0. \tag{55}$$

When conditions (32) and (33) are applied, the first terms in the left-hand sides of Eqs. (54) and (55) can be neglected. Thus, these equations can be transformed into

$$\eta_0' = -\frac{\alpha\beta^2}{2(1+\alpha^2)}\sin\eta_0 \cos\eta_0 \tag{56}$$

and

$$\xi_0' = -\frac{\alpha\beta^2}{2(1+\alpha^2)}\sin\xi_0 \cos\xi_0. \tag{57}$$

When

$$0 \le \xi_0 \le \pi, \quad 0 \le \eta_0 \le \pi, \tag{58}$$

Eqs. (56) and (57) possess the following equilibrium points:

$$(0; 0), \quad (0; \pi), \quad (\pi; \pi), \quad (\pi; 0); \tag{59}$$

$$\left(\frac{\pi}{2}; \frac{\pi}{2}\right); \tag{60}$$

$$\left(0; \frac{\pi}{2}\right), \quad \left(\frac{\pi}{2}; \pi\right), \quad \left(\pi; \frac{\pi}{2}\right), \quad \left(\frac{\pi}{2}; 0\right). \tag{61}$$

Eq. (59) represents the points of stability, i.e. the points-attractors; Eq. (60) represents the point-repeller; Eq. (61) represents the saddle-like points.

Eqs. (56) and (57) represent the particle trajectory equations which after being integrated can be expressed as

$$\frac{1 + \cos(2\eta_0)}{1 - \cos(2\eta_0)} = C_2 \frac{1 + \cos(2\xi_0)}{1 - \cos(2\xi_0)}, \tag{62}$$

where C_2 is an arbitrary constant. In particular, if $0 \le \eta_0(\xi_0) \le \pi/2$, Eq. (62) yields

$$\eta_0(\xi_0) = \frac{1}{2}\cos^{-1}\left[\frac{C_2 \dfrac{1 + \cos(2\xi_0)}{1 - \cos(2\xi_0)} - 1}{C_2 \dfrac{1 + \cos(2\xi_0)}{1 - \cos(2\xi_0)} + 1}\right]. \tag{63}$$

The particle drift trajectories calculated using Eq. (63) are shown in Fig. 3. The particle migration from the repelling points (empty circles) to the attracting points (filled circles) is shown by arrows. The saddle-like points are marked with a cross. It is important to stress that the shape of particle trajectories in the resonator is not affected by parameters α and β i.e. does not depend on the particle size and IGW intensity. This conclusion is suggested by the fact that the functions of the vertical and the horizontal drift components are identical with respect to α and β (see Eqs. (54) and (55)).

The non-dimensional time scale τ_* was determined using Eqs. (56) and (57) and appeared to be the same as described by Eq. (40), i.e. the mean drift velocity in the two-dimensional resonator is proportional to the square of the particle size and to the IGW intensity. The quantitative analysis shows that the IGW-caused structurization in the resonator is as slow as the vertical drift process in the waveguide.

Thus, the IGW-caused particle drift can result in the two-dimensional structurization of the two-component system (e.g., a hydrosol) in the resonator. The particle concentration increases with the time in the vicinity of the attractive points and decreases near the repelling points (see Fig. 3). It seems to be rather complex to provide an accurate analytical prediction of the

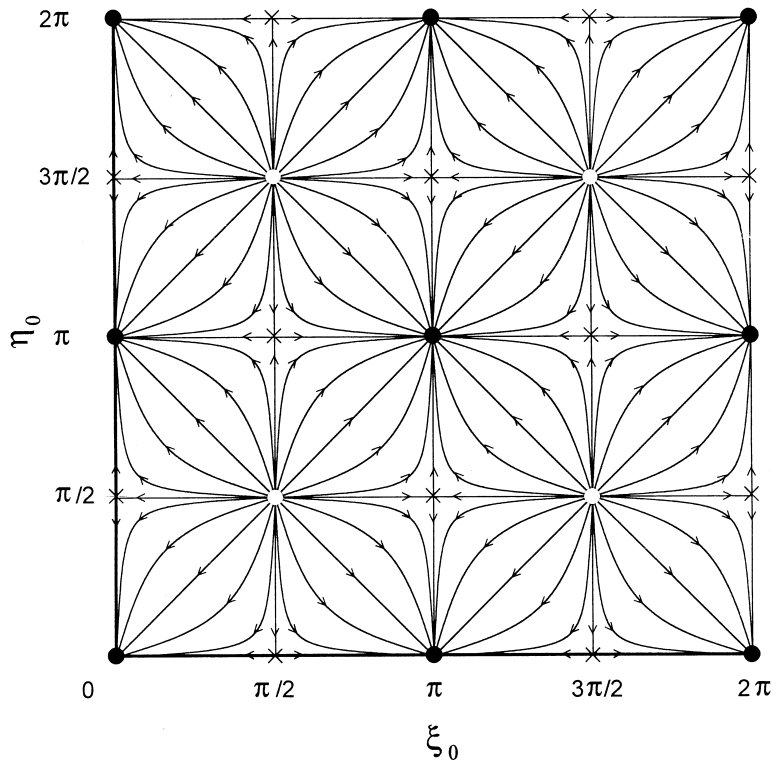

Fig. 3. Particle trajectories in the rectangular IGW resonator (analytical calculation).

particle behavior near the saddle-like points because of the non-autonomic nature of Eqs. (52) and (53).

4.2. Computer simulation

When considering the standing IGW in the resonator, the particle motion near the saddle-like points can be studied by a computer simulation. The particle motion is governed by basic non-dimensional Eqs. (52) and (53). The numerical simulations were conducted at $\beta = 10^{-1}$ and $\alpha = 10^{-3}$ and 10^{-2}. First, a single particle motion was simulated. Second, the ensemble of 1000 particles was studied.

The numerical solution of Eqs. (52) and (53), found at $\alpha = 10^{-2}$ for a single particle initially located in the vicinity of the repelling point $(\pi/2; \pi/2)$, are presented in Fig. 4. The shape of the numerically calculated trajectories represents the particle drift accompanied by their oscillating motion (the curves in Fig. 4 are not smooth like those obtained analytically and shown in Fig. 3). The arrows in Fig. 4 show that the particles migrate to the attractive points, thus decreasing the particle concentration near the repelling points. The data presented in Fig. 4 were averaged in order to eliminate the oscillation component. Based on these "averaged" trajectories, it was concluded that the particle drift trajectories in the resonator described

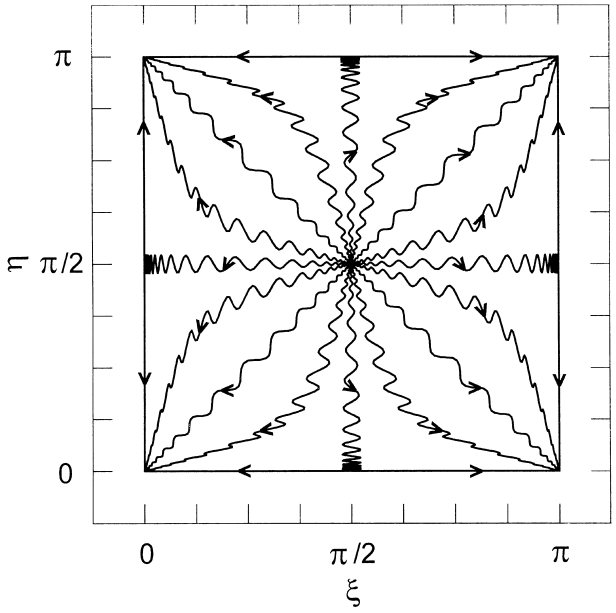

Fig. 4. Trajectories of a single particle initially located in the vicinity of the repelling point ($\pi/2$; $\pi/2$) in the rectangular IGW resonator (numerical calculation).

respectively by the numerical and analytical solutions are quantitatively the same. This conclusion was confirmed when conducting calculations with $\alpha = 10^{-3}$.

For the particle ensemble, the particle behavior was studied near the points of their concentration, i.e., the attractive and saddle-like points. The calculations started at the initial moment, $\theta = 0$, when the particles were assumed to be stochastically distributed inside the region of $2\pi \times 2\pi$ with $\xi'(0) = \eta'(0) = 0$. The patterns that represent the six time points, $\theta = 0$, 2×10^4, 5×10^4, 10^5, 2×10^5, and 4×10^5, are shown in Fig. 5. It is shown that the structure of a dispersed system changes with time, since the particles are concentrating at the attractive points of the resonator. Some particles first move to the saddle-like points (it is clearly seen at $\theta = 2 \times 10^5$) and then finally join other particles in the attractive points (seen at $\theta = 4 \times 10^5$).

The computer simulation confirms that the particle drift in the IGW field generated in two-dimensional resonator results in the particle structurization. The characteristic time of the development of the structurization process appears to take a few days ($\theta \sim 10^4$–10^5, see Fig. 5), which agrees well with Eq. (40).

5. Method for acceleration of IGW-caused structurization

The results presented above show that in practical situations the vertical drift in the infinite horizontal waveguide and the two-dimensional drift in the resonator are very slow which results in the rather slow structurization of the two-component system. This section introduces the method for the significant acceleration of the IGW-caused structurization, which utilizes

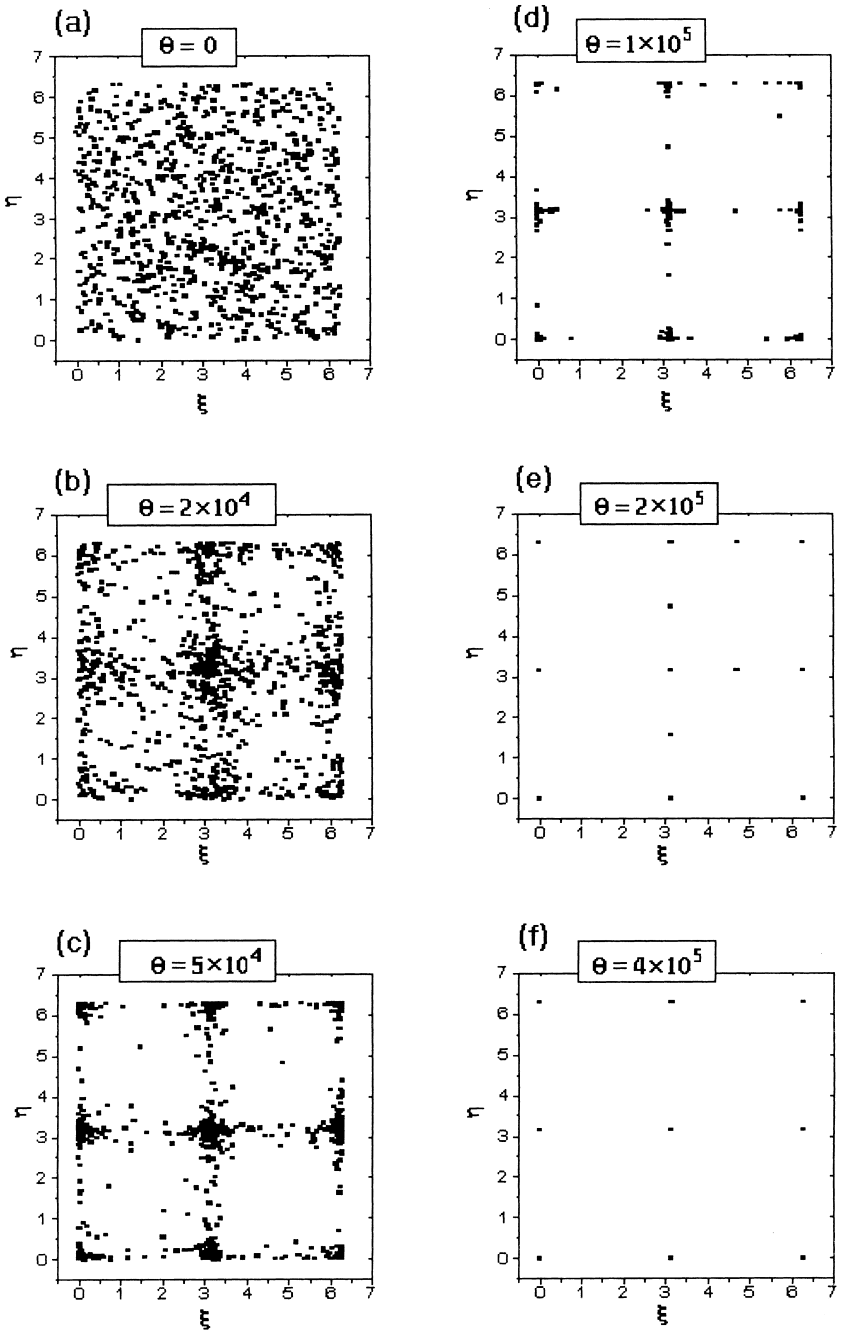

Fig. 5. Particle patterns in the rectangular IGW resonator at different time points (numerical calculations).

the horizontal component of the particle drift motion in the infinite waveguide. The horizontal drift velocity component may be relatively high, as assessed by Eqs. (43) and (27). The particles in the infinite waveguide follow the curved trajectories so that some of them move in the wake of the wave and some do in the opposite direction (see Fig. 1). When the waveguide is semi-infinite (the IGW radiator represents the "vertical boundary"), some particles move toward the radiator and deposit on its surface while other particles move away from the radiator thus purifying certain areas. This is schematically displayed in Fig. 6 which represents the case $n = 1$. The particle concentration decreases in the regions marked by symbol "1" (near the waveguide horizontal boundaries), whereas their concentration increases in the region marked as "2" (the waveguide center). The particle concentration remains essentially the same in the intermediate region "3". In the general case ($n \geq 1$), the layers of a purified fluid (total of $n+1$) will alternate with the layers loaded with particles (total of n).

Eq. (45) suggests that the lower is α (i.e. the particles size), the greater is the width of the "clean" regions. The velocity of particles moving in region "1" away from the radiator is determined primarily by the horizontal component of the drift and can be obtained using Eq. (43). If $\alpha \ll 1$, the horizontal drift velocity is estimated as

$$u_{\mathrm{d}} = \frac{\omega_n}{k}\xi_0' \sim \frac{\omega_n}{k}\frac{\beta^2}{2} \tag{64}$$

For soft isothermal water (see Lighthill, 1978)

$$\omega_n \sim N \sim 10^{-3}\ \mathrm{s}^{-1}. \tag{65}$$

Assuming $\beta = 0.1$ and of $\lambda_x \sim 10^5$ cm, the drift velocity is in the order of

$$u_{\mathrm{d}} \sim 1\ \mathrm{cm/s}. \tag{66}$$

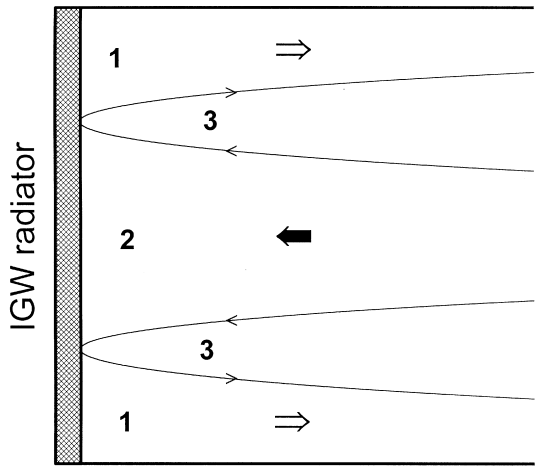

Fig. 6. Particle horizontal drift in the semi-infinite IGW waveguide (schematics).

It is remarkable that this value does not depend on the particle size and is determined only by the IGW parameters. The energy needed to purify the volume of 1 cm^3 can be evaluated as

$$\varepsilon \sim \frac{\rho_0 u_n^2 u_g}{u_d}, \tag{67}$$

where u_n and u_d are defined by Eqs. (23) and (64), respectively; u_g is the horizontal component of the IGW group velocity. If the waveguide height is $h \sim 10$ m, we estimate $k_z \sim \pi/h \sim 10^{-3}$ cm, i.e., $k_z \gg k_x \sim \pi/\lambda_x$. Utilizing the standard equation for the group velocity (Lighthill, 1978), we obtain

$$u_g \sim \frac{N}{k_z}, \tag{68}$$

Using the above indicated assumptions, we estimate that $\varepsilon \sim 10^{-5}$ J/cm^3 = 10 J/m^3, which appears to be a very low energy consumption due to the low group velocity value: $u_g \sim 1$ cm/s, see Eq. (68).

It is concluded that the semi-infinite waveguide allows us to significantly increase the structurization rate using relatively small energy resources. In addition, the model of the semi-infinite waveguide with the IGW radiator as a vertical boundary seems to be more realistic than the infinite waveguide model, since in the former one the radiator may effectively serve for the IGW excitation.

6. Discussion and conclusions

Internal gravity waves have much lower frequency and smaller group velocity compared to acoustic waves. Similarly to acoustic waves, IGWs generate the particle drift in a two-component system.

The analytical and numerical calculations of the IGW-caused particle drift were performed for the following two situations (i) the propagating IGW in the horizontal infinite waveguide and (ii) the standing IGW in the rectangular resonator. The particle trajectories in the IGW horizontal waveguide were found to be more complicated than those generated by an acoustic waveguide. Indeed, IGW causes the transverse stratificating drift accompanied by the longitudinal drift, while in the acoustic waveguide the particles migrate in the wake of the wave (King, 1934; Redcoborody, 1995). The standing IGW and the acoustic wave in the rectangular resonator feature similar particle drift characteristics.

The data on the particle drift in low-frequency standing IGW obtained in this study show a good qualitative agreement with the results obtained by Dain et al. (1995) for the particles in a two-dimensional high-frequency sonic field. One example of this similarity is the emergence of knots (attractive and repelling points) and saddle-like points. For the domain considered in the paper by Dain et al. (1995), there exists an additional side drift along the nodes and antinodes. It should be noted that both the low-frequency waves (such as IGW) and the high-frequency sonic waves may be utilized for cleaning suspensions from the particles.

As a result of the particle migration in the IGW field, the particles concentrate in the certain

areas of the field. The particle size was found to affect the shape of particle trajectories and the drift velocity in the infinite waveguide. In contrast, the shape of trajectories in the IGW rectangular resonator was found independent on the particle size and IGW intensity.

The IGW-caused particle drift may result in the partial purification of a two-component system associated with its structurization. The latter is characterized by the formation of alternating areas of the fluid: an entirely purified layer (does not contain any particles) alternates with a layer loaded with particles. These effects require a relatively low energy, about 10 $J \cdot m^3$ (much lower than that of the acoustic wave).

The particle migration for the two above indicated situations was found to be a very slow process and, therefore, the time needed for an efficient purification (or structurization) of a fluid is rather long and increases quickly with the decrease in particle size. However, the particle coagulation (not considered in this study) may significantly reduce the actual time of this process. The oscillating and drift motion favors coagulation so that this effect may be pronounced even if the initial particle concentration is relatively low. The effect of α on the particle drift rate, or in other words its particle size dependence, suggests that this phenomenon is similar to the so-called gravity coagulation (Khrgian, 1986), which is extremely efficient in warm atmospheric clouds at low aerosol concentrations. In addition, the effect of α on the amplitude of oscillation also promotes the particle coagulation.

Even if the role of the particle coagulation is neglected, the partial purification of a two-component system can still be significantly accelerated through utilizing the horizontal component of the particle drift in the semi-infinite IGW waveguide described in Section 5. In this model, the liquid fully purifies from particles near the radiator, and the area of purification expands along the waveguide with the velocity of the order of 1 cm/s (in the absence of convection).

While the IGW field was found to generate a considerable stratification, this stratification may be potentially reduced by the Brownian diffusion. Therefore, we assessed the Brownian diffusion effect as described below. The coefficient of Brownian diffusion, D, was determined by the well-known Einstein's expression (Huang, 1963):

$$D = \frac{k_b T}{6\pi\rho\nu R_p}, \tag{69}$$

where k_b and T are the Boltzman constant and the temperature, respectively. The characteristic time τ_d of the particle diffusion motion to the distance S was estimated as

$$\tau_d = \frac{S^2}{D} = \frac{S^2 6\pi\rho\nu}{k_b T} R_p. \tag{70}$$

The characteristic time τ_* of stratification under IGW was determined from Eq. (40) as

$$\tau_* \sim \frac{1}{\alpha\beta^2} = \frac{9\rho\nu}{2\omega^2\rho_p\beta^2}\frac{1}{R_p^2}. \tag{71}$$

Thus, τ_d increases with the increase of R_p while τ_* decreases at the same time. Assuming that $\omega \sim 0.1\ s^{-1}$, $\beta \sim 0.1$, $S \sim 10$ m, we conclude that the equality of $\tau_d = \tau_*$ may occur in water if the size of suspended particles is $R_p \sim 0.1$ μm. For the larger particles, $\tau_d > \tau_*$. This estimation

shows the Brownian diffusion is insignificant, at least, for the space scales of $S > 10$ m. Also, the Brownian diffusion cannot make the stratification quickly disappeared with time once the wave field is shut down: for the above indicated conditions, the IGW-generated stratification may essentially dissipate in about 10^6 years.

The IGW-caused particle drift may play a significance role in many natural processes occurring in large water reservoirs with low convection and thus may be of interest for atmospheric and oceanic research.

Acknowledgements

This study was supported by the Government of Sweden through Collaborative Project 312 with the Science and Technology Centre in Ukraine and by the NATO Scientific and Environmental Affairs Division through Collaborative Research Grant ENVIR.CRG.961120. The authors deeply appreciate this support.

References

Batchelor, G.K., 1967. An Introduction to Fluid Dynamics. Cambridge University Press, Cambridge 758.

Bergman, L., 1957. Ultrasonics and its Application in Science and Technology. IIL Press, Moscow, p. 726 (in Russian).

Dain, Y., Fishman, M., Gutfinger, C., Pnueli, D., Vainshtein, P., 1995. Dynamics of suspended particles in a two-dimensional high-frequency sonic field. J. Aerosol Sci 26, 575–594.

Duhin, S.S., 1960. Drift theory for an aerosol particle in a standing acoustic wave. Kolloidny Zhurnal 22, 128–130 (in Russian).

Gossard, E., Hooke, H., 1975. Waves in Atmosphere. Elsevier, New York, p. 532.

Huang, K., 1963. Statistical Mechanics. Wiley, New York, London 520.

Kapitza, P.L., 1951. Dynamic stability of a pendulum with oscillating hanger point. J. Experimental and Theoretical Physics 21, 588–597.

King, L.V., 1934. On the acoustic radiation pressure on sphere. Proc. Roy. Soc A147, 215–225.

Khrgian, A.K., 1986. Physics of Atmosphere. Moscow University Press, Moscow, p. 328 (in Russian).

Landau, L.D., Lifshitz, E.M., 1986. Hydrodynamics. Science, Moscow, p. 736 (in Russian).

Lighthill, J., 1978. Waves in Fluids. Cambridge University Press, Cambridge, p. 588.

Mednikov, E.P., 1963. Acoustic Coagulation and Precipitation of Aerosols. Academy Press, Moscow, p. 263 (in Russian).

Priest, E., 1984. Solar Magneto-Hydrodynamics. Reidel, Dordrecht-Boston-Lancaster, p. 469.

Redcoborody, Y.N., 1995. On the theory of the small particle drift in acoustic fields. Preprint 95-2P, Main Astronomic Observatory, Kyiv, 48 p. (in Russian).

Stevenson, T.N., 1973. The phase configuration of internal waves around a body moving in a density stratified fluid. J. Fluid Mech 60 (4), 759–767.

Vainstein, P., Fishman, M., Pnuei, D., 1992. On the drift of aerosol particles in sonic fields. J. Aerosol Sci 23, 631–637.

Westervelt, P.J., 1950. The mean pressure and velocity in a plane acoustic wave in a gas. J. Acoust. Soc. Amer 22, 319–327.